Martijn Vlaar
Biomedical Engineering: Biomechatronics
Student number: WB1222457
Department number: 1192
February 13th, 2012

Targeted brain activation using isometric motor tasks during functional magnetic resonance imaging

Martijn P. Vlaar[1], Winfred Mugge[1], Paul F.C. Groot[2], Frans C. T. van der Helm[1,3], Anne-Fleur van Rootselaar[4], and Alfred C. Schouten[1,3]

[1]Department of BioMechanical Engineering, Delft University of Technology, 2628 CD Delft, The Netherlands, [2]Department of Radiology, Academic Medical Center, P.O. Box 22660, 1100 DD Amsterdam, The Netherlands, [3]Laboratory of Biomechanical Engineering, MIRA Institute for Biomedical Technology and Technical Medicine, University of Twente, 7500 AE Enschede, The Netherlands, and [4]Department of Neurology and Clinical Neurophysiology, Academic Medical Center, P.O. Box 22660, 1100 DD Amsterdam, The Netherlands

Over 0.9% of the population suffers from a movement disorder. The pathophysiology of most movement disorders remains unknown, thereby impairing effective diagnosis and consequently effective treatment. Abnormal activity of the cerebellum (CBL) and basal ganglia (BG) has been implicated in many movement disorders, including Parkinsonian tremor and dystonia. Selectively activating these brain regions may help identify pathological changes and expedite diagnosis. Dedicated pairs of isometric wrist flexion tasks with and without visual feedback of the exerted torque were devised to selectively activate the CBL and BG in healthy subjects (N=5), while ensuring safety and keeping artifacts to a minimum. Increased activity in CBL and BG (putamen) was found during a constant torque task with visual feedback compared to a constant torque task without visual feedback. Increased BG (caudate nucleus) activity was found when comparing a torque task with visual feedback where flexion and rest were rapidly alternated, to the same task without visual feedback. Increased activity in the CBL was found during a constant torque task with visual feedback with an added visual error compared to a constant torque task with normal visual feedback. This study shows that specific pairs of motor tasks using the wrist and simple MR-compatible equipment allow for targeted activation of CBL and BG and paves the way for more extensive research and eventually improved diagnosis of patients.

Introduction

Human motor control

The human body is able to perform fast, accurate and efficient motor actions and is able to correct for perturbations while performing these actions. The central nervous system (CNS) is responsible for the execution of voluntary as well as involuntary actions like reflexes using a framework of multiple interconnected control loops. This framework includes the cerebellum (CBL) and basal ganglia (BG). The CBL integrates sensory information and concerns the unconscious neuromuscular control of a joint (Hagert, 2010), which includes correcting for errors (Afifi and Bergman, 2005). BG is a collective term for a group of brain parts including the caudate nucleus, putamen and globus pallidus. The role of the BG in motor control is less apparent. They are supposedly involved in the control of complex patterns of motor activity (Hendelman, 2006). When one of the components of the framework is impaired, then the functioning of the control loops is affected which results in movement disorders.

Movement disorders

Movement disorders impair the ability to produce and control bodily movements (Chou et al., 2012), resulting in immobility and social inconvenience (Grimaldi and Manto, 2010). Over 0.9% of the population suffers from a movement disorder (Louis and Ferreira, 2010). There are several types of movement disorders most of which still have an unknown pathophysiology. Movement disorders are therefore currently often diagnosed by symptoms. Each movement disorder requires specific treatment so accurate diagnosis is essential. Unfortunately, diagnosis of movement disorders is hindered by the similarity of their symptoms. An incorrect diagnosis could not only lead to ineffective treatment, but also to adverse consequences (Findley et al., 1981). Developing tools to aid physicians diagnose patients with movement disorders may facilitate effective treatment by early detection and improved accuracy of the diagnosis.

Examples of movement disorders originating in the CNS are tremor and dystonia. There are over ten types of tremor (Rubchinsky et al., 2007) of which the main symptom is a rhythmic involuntary oscillatory movement of body parts (Harish et al., 2009). An example of tremor is Parkinsonian tremor associated with Parkinson's disease, in which the BG are found to be hypoactive based on models and brain-imaging studies (Yu et al., 2007). The CBL can be hyperactive (Rascol et al., 1997, Wu and Hallett, 2005) and hypoactive (Turner et al., 2003) in Parkinson's disease, which

may depend on the type of sensory feedback available to the patient under study. It remains unclear whether the altered CBL activation is a consequence of the pathophysiology of Parkinson's disease or whether it is a compensatory response to the hypoactive BG. Abnormal BG activity is also found in dystonia, a condition characterized by muscle contractions that cause twisting and repetitive movements or abnormal postures (Friedman and Standaert, 2001). Several studies found hypoactivity in the BG in patients with dystonia (Lozano et al., 1997, Vitek et al., 1999). Hutchison et al. (2003) demonstrated that the previously found hypoactivity was caused by the use of medication during research and that proprioceptive sensory information is underrepresented in the BG in patients with dystonia. In contrast, Peller et al. (2006) found hyperactivity in the BG in writer's cramp, a focal dystonia of the hand. These examples illustrate the difficulties in understanding the pathophysiology of movement disorders.

Problem statement and goal

Studying activations in the CBL and BG during the execution of motor tasks and comparing results between healthy subjects and patients with certain movement disorders will help identify pathological changes associated with those movement disorders. Functional magnetic resonance imaging (fMRI) is a non-invasive technique for visualizing neural activity, which enables imaging of deep brain structures like the BG. The downside to using fMRI is its sensitivity to image distortions due to movement of the subject's head (Thulborn, 1999) and to the use of magnetic or conductive materials. Magnetic materials are attracted to the MR scanner, which presents a threat to safety and affects the homogeneity of the MR scanners magnetic field deteriorating image quality (Tsekos et al., 2007). Conductive materials that are moved in the MR scanner's magnetic field cause eddy currents, resulting in heating of the material and a magnetic field that affects the homogeneity of the MR scanners magnetic field (Tsekos et al., 2007). Creating a paradigm using a pair of subtly different motor tasks and analyzing the recorded fMRI data enables visualization of differences in brain activation between these tasks. Patients can show CBL or BG activity when it is not expected (hyperactivity), or show no CBL or BG activity when it is expected (hypoactivity).

Therefore, using fMRI to achieve a better understanding of movement disorders requires a measurement paradigm to consistently activate the CBL and BG and an MR-compatible measurement setup that enables the execution of motor tasks without causing motion artifacts.

The goal of this research is to selectively evoke brain activity in the CBL or BG using isometric motor tasks, and to verify this using an MR-compatible force sensor during brain imaging using fMRI in healthy subjects.

CBL and BG activity in isometric motor tasks

Increased CBL and BG activity is expected in motor tasks where additional feedback is provided, since feedback allows for corrective actions which in turn require complex motor actions. The number of studies that investigate brain activation in the CBL and BG during motor tasks with feedback is limited. Hidler et al. (2005) did not find activity in the CBL or BG when comparing a task where a healthy subject relaxed to an isometric wrist torque task where the subject switched from exerting a certain torque with visual feedback to relaxing and back at 1 Hz. This finding suggests that a fast switching task will be executed using feed-forward control. On the other hand, Vaillancourt et al. (2003) did find activity in the CBL and BG (putamen) in healthy subjects when comparing a grip force task with visual feedback to the same task without visual feedback. Visual feedback appears to facilitate adaptation of the subject's motor commands during the task. Klarhöfer et al. (2007) found activity in the CBL in healthy subjects when comparing a gripping task with visual feedback to the same task with force perturbations generated using a haptic manipulator. Increased activation in both CBL and BG, only CBL, and in neither CBL nor BG has been demonstrated using isometric motor tasks during fMRI.

Limitations of performed studies

Some studies resolved motion of the head by presenting the subject with visual feedback of the head position, requiring the subjects to self-stabilize their head (Vaillancourt et al., 2003, Yu et al., 2007). This method of head motion reduction was demonstrated by Thulborn (1999), however it was only validated for eye movement paradigms. Many studies used conductive materials in their setup for force measurement, constructions and data transfer (Hidler et al., 2005, Klarhöfer et al., 2007, Haller et al., 2009, Hribar et al., 2009). Coombes et al. (2010) amplified visual feedback of the subject's own force error to provoke corrective action in an isometric grip force task, inducing inter-subject variability of the disturbance signal. During motor tasks in fMRI, task-related visual feedback is most common, although tactile and auditory feedback have been used (Ehrsson et al., 2000, 2001). Previous research studied brain activation during motor tasks performed on various limbs, with various feedback modalities, on several brain regions with minimal sets of tasks.

Approach
Dedicated pairs of motor tasks were devised to selectively activate the CBL and BG, while ensuring safety and keeping artifacts to a minimum. The motor tasks were executed using flexion torque of the wrist, since the wrist is often affected in movement disorders and since it is easily accessible when a subject is in the MR scanner. Movement was kept to a minimum by using isometric motor tasks. The torque sensor was mounted on a lower arm support which was attached to the right forearm of a subject (see Figure 1). The advantages of attaching the sensor structure to the subject's lower arm instead of to the MR scanner bed were twofold: Firstly, the device could be mounted outside of the MR scanner room thereby saving costly time occupying the MR scanner room. Secondly, subjects did not exert forces to their surroundings, reducing head motion.

Hypotheses
The following hypotheses were formulated:

1. Comparing a constant torque task with visual feedback to the same task without visual feedback will result in increased activity in the CBL and BG since motor actions will be adapted (more) when there is visual feedback.
2. Comparing a fast switching torque/rest task (1 Hz) with visual feedback to the same task without visual feedback will result in no increased activity in the CBL and the BG since both tasks are too fast to correct for errors and will be performed using feed-forward control.
3. Comparing a constant torque task with visual feedback and visual perturbations to the same task without visual perturbations will result in increased activity in the CBL since corrections are necessary to maintain the desired torque level.

Methods

Subjects
Five subjects (3 men), all right-handed with a laterality index greater than 70 according to Edinburgh Handedness Inventory (Oldfield, 1971) and aged between 25 and 30, were included and provided written informed consent prior to participation in this study, which was approved by the medical ethics committee of the Academic Medical Center Amsterdam. Exclusion criteria were: metal parts in body, claustrophobia, reluctance to be informed about observed abnormalities in MR images, pregnancy, known psychiatric history, known neurological conditions, use of centrally active medication, substantial daily use of alcohol (>2 units per day) or drugs, and use of alcohol or drugs within 24 hours before participation in the research.

Equipment
An MR-compatible torque sensor without magnetic and conductive materials was developed to ensure safety and reduce artifacts (see Appendix A). Torque was measured using light intensity measurements on a deformable body inside the MR scanner room while all electronics were located in the MR control room. Torque data was acquired and processed using MATLAB (MathWorks, Natick, MA.). The right forearm of the subject with attached torque sensor was placed on a sandbag alongside the body without the right forearm touching the hip. The 3T MR scanner (Philips Intera, Best, The Netherlands) was equipped with a visual information system using a mirror, a projection screen and a beamer, which presented the subject in the MR scanner with task-related information (see Figure 2).

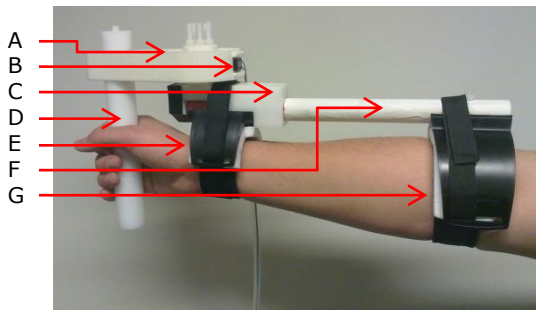

Figure 1 Torque sensor with arm support, which consisted of a polyamide 12 deformable body [A], light intensity sensor with 10m optical fiber [B], polyoxymethylene mounting block [C], polyoxymethylene handle [D], plastic armrests [E&G] with moldable foam and Velcro straps and fiberglass rod [F].

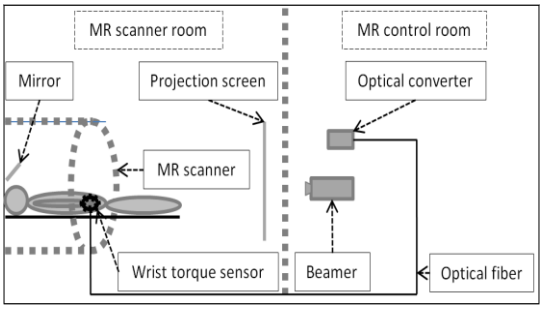

Figure 2 Schematic setup of the experiment. The subject was positioned inside the bore of the MR scanner with his right arm (with attached torque sensor) beside his body.

An anatomical scan was acquired using a resolution of 0.875x0.875 mm and a slice thickness of 1.2 mm. The 356 functional scans were acquired using: echo planar imaging, TR=3 s, TE=75 ms, resolution of 2.29x2.29 mm and a slice thickness of 3 mm. Settings were optimized for fast-paced functional scans of the CBL, BG and the majority of the cortical motor areas, which include the pre-supplementary motor area, supplementary motor area, premotor cortex, and primary motor cortex. A part of the orbitofrontal cortex was not scanned.

Tasks

Four conditions that comprise seven tasks were performed to test the hypotheses. Prior to the experiment subjects received instructions and practiced the tasks to account for learning effects. Each task was performed 3 times and consisted of 5 s visual instruction (see Appendix B) and 35 s task execution. The tasks were presented in 3 consecutive series of 7 randomly ordered tasks. All subjects performed a warm-up of which the data was discarded. The required wrist flexion torque was 0.75 Nm, which was roughly 4 to 8% of the maximum voluntary contraction. The torque sensor was set to zero at the start of the experiment while the subject was holding the handle to remove passive torque. The subjects were instructed to keep their fingers gripped around the handle during all tasks.

- *Rest condition*
  - Task 1: Rest task where the subject was instructed to relax. The projection screen was blank.
  - Task 2: Rest task where the subject was instructed to watch the projection screen and to exert no torque. The projection screen showed a visual stimulus in the form of a constant target torque and a torque indicator moving similarly to one in other tasks with visual feedback.
- *Fast switching torque condition*
  - Task 3: Fast switching torque task where the subject was instructed to alternately relax and exert the amount of flexion torque as indicated by the target on the projection. The exerted torque was also presented on the screen (visual feedback). The target switched from 0 to 0.75 Nm and back at 1 Hz.
  - Task 4: The same as task 3 but without visual feedback. The projection screen only showed the switching target torque, hence the torque amplitude had to be exerted from memory.
- *Constant torque condition*
  - Task 5: Constant torque task where the subject was instructed to match the target torque of 0.75 Nm on the projection screen with visual feedback.
  - Task 6: The same as task 5 but without visual feedback. The projection screen only showed the target torque, hence the torque amplitude had to be exerted from memory.
- *Constant torque condition with visual disturbance*
  - Task 7: The same as task 5 but a disturbance signal was added to the visual feedback of the exerted torque, provoking compensatory action from the subject (McRuer and Jex, 1967). The disturbance signal was a multisine (Pintelon and Schoukens, 2001) with a maximum amplitude of 0.075 Nm consisting of ten frequencies between 0.1 and 3 Hz and a logarithmically decaying power (-40 dB over the full frequency range).

Analysis

The recorded torque data was inspected to assess when a subject started to perform the task correctly, resulting in at least 22 seconds of data. The following criteria were used: in conditions 1 and 3 the exerted torque level had to be settled, in condition 2 the torque had to be exerted at 1 Hz and in condition 4 the disturbance had to be successfully followed. The SPM8 (Statistical Parametric Mapping) software package was used to preprocess the functional data, specify the model and perform the statistical analysis (see Appendix C). The fMRI results of the entire scanned portion of the brain were analyzed on group level using an uncorrected significance level of $p=0.001$ and a 5 extent cluster threshold.

The result of performing a statistical analysis on a pair of tasks was a map of voxels indicating brain regions active during one task and inactive during the other, and vice versa. The following maps of active brain regions were generated:

- Brain regions showing increased activity during the constant torque task with visual feedback (task 5) compared to during the constant torque task without visual feedback (task 6). This comparison was abbreviated to **5vs6** and the opposite comparison was abbreviated to **6vs5**.
- Brain regions showing increased activity during the fast switching torque task with (task 3) compared to during the fast switching torque task without visual feedback (task 4). This comparison was abbreviated to **3vs4** and the opposite comparison was abbreviated to **4vs3**.
- Brain regions showing increased activity during the constant torque task with visual feedback and visual disturbance (task 7) compared to during the constant torque task with visual feedback and without visual disturbance (task 5). This comparison was abbreviated to **7vs5** and the opposite comparison was abbreviated to **5vs7**.

Increased CBL and BG activity was expected when testing 5vs6 (hypothesis 1). The same level of CBL and BG activity was expected when testing 3vs4 and 4vs3 (hypothesis 2). Increased CBL activity was expected when testing 7vs5 (hypothesis 3). Change in activity was not expected to be limited to the CBL and BG. When testing 5vs6 and 3vs4 increased activity in the visual cortex was expected. Since there was no visual feedback during task 4 and task 6 the torque level had to be reproduced from memory, consequently activity was expected in brain regions responsible for memory retrieval when testing 4vs3 and 6vs5. The error corrections from the CBL are processed by the cortical motor areas (Pockett et al., 2006). These brain regions were expected to show increased activity when testing 5vs6 and 7vs5, since in these comparisons increased error corrections coming from the CBL were expected. Increased activity during task 2 (visual stimulus during rest) compared to during task 1 (rest) was predicted in brain regions responsible for visual processing. This comparison was included to verify the approach and subsequent statistical analysis using a robust paradigm. Functionally scanning the bulk of the brain allowed for verification of the predicted increases in activation, as well as reviewing unpredicted increases in activation throughout the brain.

Since no magnetic or conductive materials are used in the MR scanner room, the only possible source of artifacts is movement of the subject's head while scanning. It is not possible to quantify the impact of the movement on the quality of the fMRI data. An indication of the amount of head movement can however be extracted from the translations and rotations (6DOF) required to achieve anatomical alignment of all functional scans to the first functional scan. Translations smaller than 1 voxel dimension (2.29mm) and rotations smaller than 1 degree are widely accepted boundaries and should have little impact on the quality of the fMRI data.

Results

Task performance

In 10 out of 15 occurrences subjects overestimated the required torque levels in the constant torque task without visual feedback (task 6) and thus exerted too much torque (see Table 1). Overestimation of the required torque also occurred during the fast switching torque task without visual feedback (task 4). For 3 out of 5 subjects the exerted torque during task 4 was beyond the 1.5 Nm capability of the torque sensor.

Table 1 Shows per subject the torque (mean and standard deviation) exerted during the three repetitions of motor task 6 (constant torque without visual feedback).

Subject	Mean torque during task 6 [Nm], goal was 0.75Nm
1	0.87(0.05), 0.74(0.10), 0.89(0.03)
2	0.71(0.03), 0.73(0.02), 0.91(0.06)
3	0.93(0.03), 1.12(0.03), 0.75(0.02)
4	1.03(0.10), 0.86(0.06), 0.68(0.04)
5	1.13(0.01), 1.19(0.05), 1.08(0.03)

Movement during functional scans

All translations were within 2.29mm, however there were subjects with head rotations exceeding 1 degree (see Table 2).

Table 2 Maximum absolute translations and rotations necessary for anatomical realignment of the 356 functional scans. x-direction: lateral (left to right), y-direction: posterior to anterior, z-direction: inferior to superior, pitch: rotation about x-axis (nodding yes), roll: rotation about y-axis, and yaw: rotation about z-axis (shaking no).

Subject	Maximum absolute translation			Maximum absolute rotation		
	x [mm]	y [mm]	z [mm]	roll [deg]	pitch [deg]	yaw [deg]
1	0.51	0.21	0.74	0.87	0.45	0.27
2	0.71	0.17	0.69	0.37	0.45	1.02
3	0.38	0.67	1.23	0.47	0.76	0.32
4	0.68	0.41	1.31	0.62	1.92	1.15
5	0.74	0.37	1.37	1.09	0.46	0.26

The Δtranslation (resultant translation of the head between sequential functional scans) between sequential scans (see Figure 3) shows that subject 3 made sudden movements during the 5s periods of instruction for each task and also during task 1 and 2. All of the translations between sequential functional scans larger than 0.13 mm/scan were during instruction and rest.

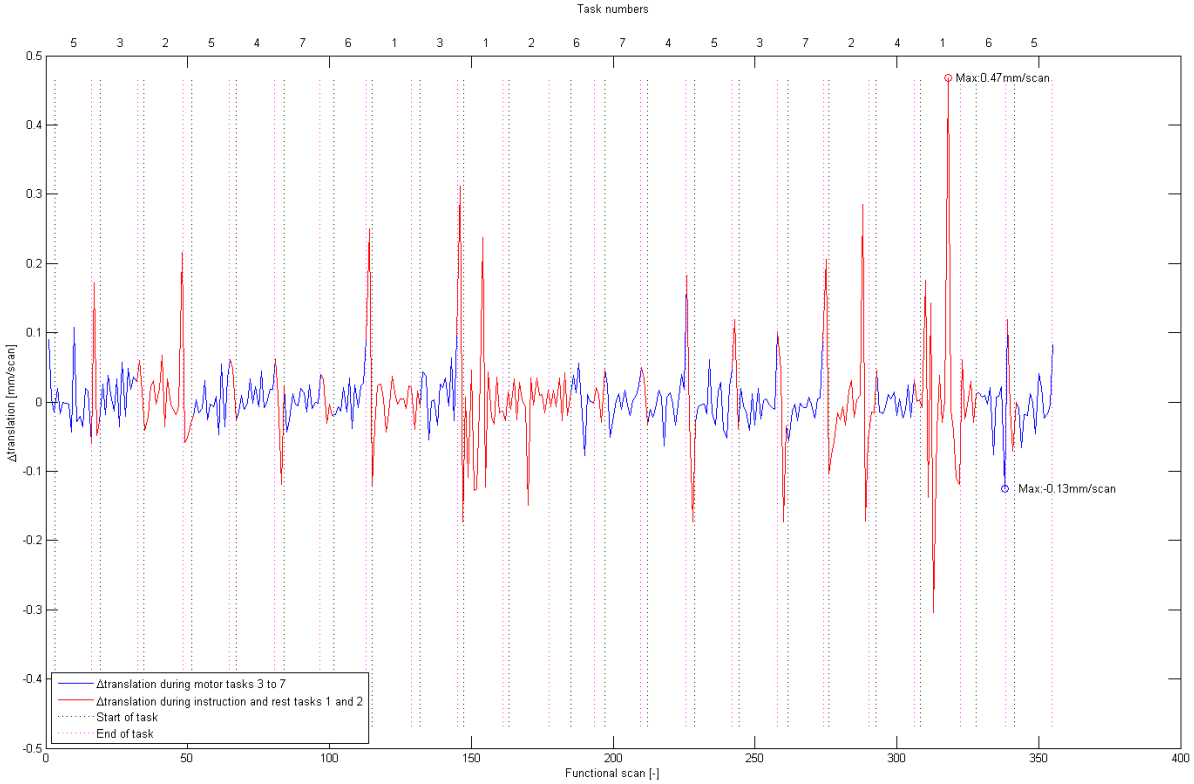

Figure 3 Δtranslation (resultant translation of the head between sequential functional scans) for subject 3. Shown on top are the task numbers indicating which task was executed during which functional scan. Vertical black dotted lines indicate the start of the task and vertical magenta dotted lines indicate the end of the task. The maximum Δtranslation [mm/scan] is indicated for the instruction and rest tasks (red circle) and for the motor tasks (blue circle). Most head displacement occurred during rest and instruction.

fMRI results

Figure 4 to Figure 6 show the results of a random-effects group analysis performed on the three pairs of tasks (N=5, p=0.001, T=7.1732, 5 voxel extent threshold). No significant brain activity was found in 5vs7. The anatomical data is derived from the active voxel coordinates using xjview8.4 and AAL, which are SPM8 extensions using the MNI (Montreal Neurological Institute) single subject anatomical brain map. Details of activated clusters can be found in Appendix D.

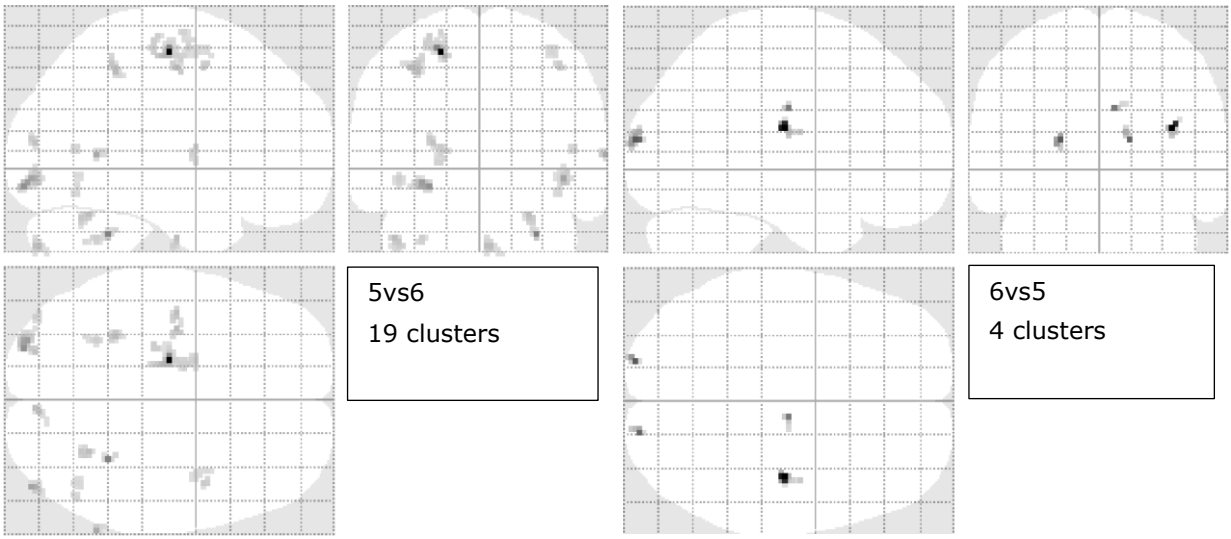

Figure 4 Clusters of active voxels in the brain resulting from comparisons between task 5 (constant torque with visual feedback) and task 6 (constant torque without visual feedback).

Clusters of active voxels in 5vs6 (see Figure 4) were found in the CBL posterior lobe, CBL anterior lobe, BG (putamen), inferior temporal gyrus, occipital lobe, superior temporal gyrus, middle temporal gyrus, inferior parietal lobule, precentral gyrus (primary motor cortex) and middle frontal gyrus. 6vs5 (see Figure 4) resulted in clusters of active voxels in the occipital lobe, insula and cingulate gyrus.

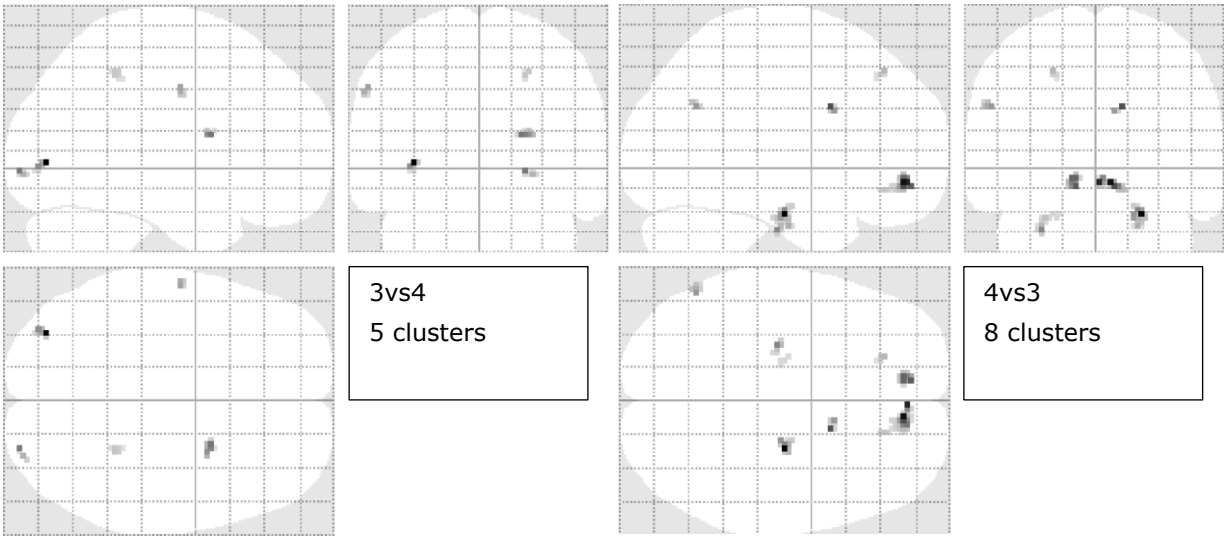

Figure 5 Clusters of active voxels in the brain resulting from comparisons between task 3 (fast switching torque with visual feedback) and task 4 (fast switching torque without visual feedback).

3vs4 resulted in clusters of active voxels in the occipital lobe, BG (caudate nucleus), precentral gyrus (primary motor cortex) and postcentral gyrus (primary somatosensory cortex). The clusters of active voxels in 4vs3 are located in the parahippocampal gyrus, frontal orbital lobe, cingulate gyrus, supramarginal gyrus and superior frontal gyrus (see Figure 5).

Clusters of active voxels in 7vs5 were found in CBL anterior lobe, middle and superior temporal gyrus, anterior cingulate, Brodmann area 8 and supplementary motor area (see Figure 6).

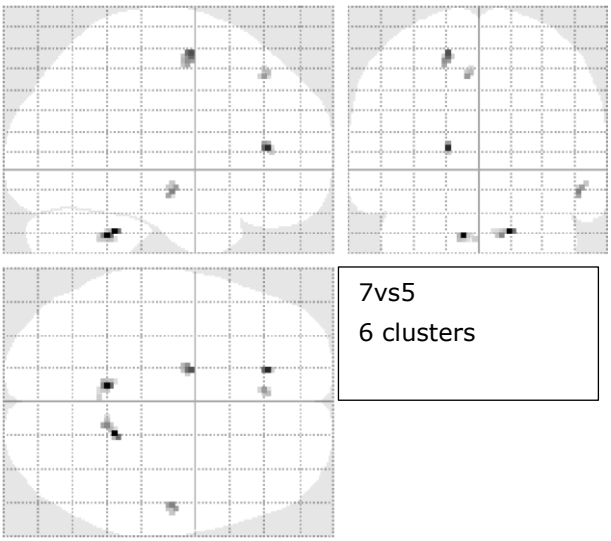

Figure 6 Clusters of active voxels in the brain resulting from comparison between task 7 (constant torque with visual feedback and visual disturbance) and 5 (constant torque with visual feedback).

Discussion

Effect of visual stimulus during rest

Brain regions that showed increased activity during task 2 (visual stimulus during rest) compared to during task 1 (rest) included the occipital lobe, inferior temporal gyrus, inferior parietal lobule, middle temporal gyrus, precuneus and middle frontal gyrus (results not shown). These brain regions are directly associated with visual processing (Martin, 2003). In agreement with the expectations and thereby verifying the approach, adding a visual stimulus to a rest task resulted in increased activity in brain regions responsible for visual processing.

Hypotheses

Indeed CBL and BG (putamen) activity was found in 5vs6 as hypothesized (hypothesis 1), which is in agreement with Vaillancourt et al. (2003), who found CBL and BG (putamen) activity comparing an isometric grip task with visual feedback to an isometric grip task without visual feedback. CBL activity was found in 7vs5 (hypothesis 3), which is in accordance with Klarhöfer et al. (2007), who found CBL activity in a task where corrective action was required, although they used a complex haptic manipulator to achieve this result. Interestingly, BG (caudate nucleus) activation was found in 3vs4 which was not expected (hypothesis 2), albeit in another part of the BG than in 5vs6.

Brain functions of active clusters

Little is known about the functions of the individual components of the human brain. An attempt will be made to identify the functions of the active brain regions using literature. The findings will be discussed per comparison as presented in the methods: 5vs6, 6vs5, 3vs4, 4vs3 and 7vs5.

The active brain regions in 5vs6 indeed included CBL, BG, cortical motor areas (primary motor cortex) and regions responsible for visual processing (occipital lobe and inferior temporal gyrus). There was also increased activity in the inferior parietal lobule, which is believed to be involved in integrating sensory information (Martin, 2003, Afifi and Bergman, 2005) and is explainable in the context of the compared tasks. Unpredicted activity was also found in the middle frontal gyrus and more specifically in the right frontal eye field (Nielsen, 2003). The frontal eye field triggers intentional saccades to visible targets or to the location where it is predicted that the target will appear (Afifi and Bergman, 2005). This increase in activation can be understood in terms of the added visual feedback during task 5. Other brain regions showing unpredicted activity were the middle and superior temporal gyri, which are primarily associated with auditory processing (Hendelman, 2006). However, another function ascribed to these gyri is contributing to smooth pursuit movements using visual information (Martin, 2003, Afifi and Bergman, 2005). The middle and superior temporal gyri also showed increased activity in 7vs5, which as 5vs6 required smooth pursuit based on visual information, therefore this is a consistent finding.

The insula showed increased activity in 6vs5 and has been implicated in memory retrieval (Ghaem et al., 1997). A brain region responsible for visual processing (another part of the occipital lobe) also showed increased activity, which may result from the absence of moving objects on the screen leaving only a static target, which is unique to motor task 6. Unpredicted increased activity was

found in the cingulate gyrus, which was also found to be active in 4vs3. The activation of the cingulate gyrus will be discussed in the next section.

As expected the active brain regions in 3vs4 included those responsible for visual processing (occipital lobe). Unexpected increase in activity was found in brain regions responsible for sensory reception (primary somatosensory cortex) and in the primary motor cortex. Perhaps, these regions are active because of the visual feedback, which in this case does not allow for continuous unconscious error correction as in 5vs6, but rather allows for conscious adjustment of wrist torque for the next occurrence of exerting the target torque. Another unexpected increase in activity was found in the body of the caudate nucleus, a part of the BG believed to be involved in learning when visual feedback is present (Seger and Cincotta, 2005). The body of the caudate nucleus has also been implicated in the oculomotor loop, which plays a role in saccadic eye movements (Martin, 2003). Both options are plausible given the nature of the compared tasks and cannot be verified based on this study.

The active brain regions in 4vs3 included as expected regions responsible for memory retrieval, namely the parahippocampal gyrus (Maguire and Mummery, 1999). Several brain regions involved in sensory and motor processing showed increased activity. These regions are the supramarginal gyrus, which has been associated with visuospatial activities (Hendelman, 2006) and the frontal orbital lobe, believed to be involved in sensory integration, learning, predicting and decision making (Kringelbach, 2005). These brain regions were not predicted to be active, but are closely related to the motor tasks at hand. Unpredicted and not easily explained activation was found in the superior frontal gyrus. The specific region of increased activity has been associated with self-related processes and was shown to become less active during a demanding fast sensorimotor processing task (Goldberg et al., 2006). So perhaps there was not an increase in activity in the superior frontal gyrus during task 4, but rather a decrease of activity during task 3 due to the complexity of the task, resulting in suppression of self-related processes. Unpredicted increase of activity was also found in the cingulate gyrus, which was as found to be active as well in 6vs5. The activation of the cingulate gyrus will be discussed in the next section.

In agreement with the expectations active brain regions in 7vs5 included the CBL and cortical motor area's (supplementary motor area). Increase of activity was found in middle and superior temporal gyri as was found in 5vs6 and has been discussed. Another brain region that showed unpredicted increase in activity was the anterior cingulate, which is believed to integrate input from various sources and contribute to the modulation of processing in other brain regions (Bush et al., 2000). This increased activity is probably explained by the added visual disturbance, requiring constant integration of sensory information and modulation of actions. Lastly activity was found close to the mesial Brodmann area 8, which has been associated with the management of uncertainty and more specifically shows increased activation when a subject experiences uncertainty (Volz et al., 2005). The unpredictability of the used disturbance signal probably contributed to this activation. The integration of sensory information and uncertainties in sensory feedback are known to play an important role in motor control (Van Beers et al., 2002, Kording and Wolpert, 2004).

Unexpected increase of activity in brain regions could largely be explained by the paradigm in which the increase occurred.

Discussion other observations

Table 2 shows the maximum translations and rotations needed to align the functional scans anatomically. Some subjects rotated their heads more than 1 degree during the functional scans, which is too much according to the rule of thumb (less than 2.29 mm and less than 1 degree). Figure 3 shows the Δtranslation between sequential functional scans for a typical subject. The sudden movement during instruction and rest suggests that subjects tried to reposition themselves between performing motor tasks, perhaps to assume a more comfortable position. These movements affect the maximum translations (Table 2), whereas they do not necessarily corrupt the fMRI results as they do not occur during tasks of interest. One could argue that it is not so much the maximum translations and rotations which determine the quality of the data, but rather the amount of translation and rotation between sequential scans. Movement between sequential scans can be corrected by anatomically aligning the separate scans, however movement during the acquisition of one scan cannot be corrected. Therefore it is probably better to regard scans that had excessive inter-scan (hence probably also intra-scan) movements as compromised.

Overestimation of the required torque level when there is no visual feedback as seen in Table 1 is a common finding (Shergill et al., 2003, Mugge et al., 2009). Both in task 4 and task 6, the two tasks without visual feedback, the exerted torque levels were higher than the required 0.75 Nm. Increase in torque level has been associated with increase in fMRI intensity in active voxels (Dai et al., 2001) or with an increased number of activated voxels in the region (Thickbroom et al., 1998).

Effects can extend to the primary motor cortex, sensory regions, supplementary motor area, premotor, prefrontal, parietal and cingulate cortices, and cerebellum (Dai et al., 2001). Therefore, some of the unpredicted increased activity in clusters in 6vs5 and 4vs3, for example in the cingulate gyrus, might be due to the higher torque level as a consequence of the overestimation of the required torque in task 6 and task 4.

During the fast switching torque tasks (task 3 and task 4) the exerted torque level did not return to zero after a torque was exerted. This effect could be caused, yet not exclusively, by the somewhat sluggish relaxation of the polymer deformable body of the torque sensor after the load is removed. Both the deactivation dynamics of the muscles and the anticipation of the next contraction are probably also responsible for this effect.

Recommendations and added value

This study demonstrates that for a small group (N=5) selective activation of CBL and BG can be achieved using an MR-compatible torque sensor and specific pairs of isometric motor tasks at low torque levels, which should also be achievable for patients. A study on a larger group of healthy subjects and on patients is warranted to further investigate the feasibility of developing a diagnostic tool based on a comparison of CBL and BG activation between healthy subjects and patients. The unexpected increase of activity in the caudate nucleus, a part of the BG which has been associated with movement disorders, warrants exploring the possibilities of targeted activation using motor tasks.

The added value of this research is that various force tasks are combined into one study, all on a single joint. The MR-compatible equipment realized unambiguous motor task execution, through conditioning the motor task and subsequent feedback, while limiting head motion.

Conclusions

1. Light intensity measurements on a deformable body allow for torque measurements without the presence of magnetic and conductive materials in the MR scanner room.
2. Attaching the torque sensor to the arm of the subject results in acceptable head displacement during isometric motor tasks, thereby limiting head motion artifacts.
3. Adding a visual stimulus to a rest task activates brain regions involved in visual processing.
4. Pairs of low torque isometric wrist motor tasks enable targeted activation of CBL and BG:
    a. A visual error in the feedback during exertion of a constant torque activates the CBL.
    b. Providing visual feedback during a constant torque task activates the CBL and BG (putamen).

Acknowledgements

This research was conducted within the context of the Movement Diagnostic System project, which is a collaboration between the Academic Medical Centre (University of Amsterdam), Technical University Delft, University of Twente, Moog Inc., Noldus, and Twente Medical Systems International. The Movement Diagnostic System project is part of the NeuroSIPE programme, which is a sustainable community and cooperation among Dutch universities and university medical centers, with the aim to develop diagnostic tools for neurological disorders.

References

Afifi AK, Bergman RA (2005) Functional neuroanatomy: text and atlas: Lange Medical Books/McGraw-Hill.

Bush G, Luu P, Posner MI (2000) Cognitive and emotional influences in anterior cingulate cortex. Trends in Cognitive Sciences 4:215-222.

Chou KL, Grube S, Patil PG (2012) Deep Brain Stimulation. United States of America: Bang Printing.

Coombes SA, Corcos DM, Sprute L, Vaillancourt DE (2010) Selective Regions of the Visuomotor System Are Related to Gain-Induced Changes in Force Error. Journal of Neurophysiology 103:2114-2123.

Dai TH, Liu JZ, Sahgal V, Brown RW, Yue GH (2001) Relationship between muscle output and functional MRI-measured brain activation. Experimental brain research Experimentelle Hirnforschung Experimentation cerebrale 140:290-300.

Ehrsson HH, Fagergren A, Forssberg H (2001) Differential Fronto-Parietal Activation Depending on Force Used in a Precision Grip Task: An fMRI Study. Journal of Neurophysiology 85:2613-2623.

Ehrsson HH, Fagergren A, Jonsson T, Westling G, Johansson RS, Forssberg H (2000) Cortical Activity in Precision- Versus Power-Grip Tasks: An fMRI Study. Journal of Neurophysiology 83:528-536.

Findley LJ, Gresty MA, Halmagyi GM (1981) Tremor, the cogwheel phenomenon and clonus in Parkinson's disease. Journal of Neurology, Neurosurgery & Psychiatry 44:534-546.
Friedman J, Standaert DG (2001) Dystonia and its disorders. Neurologic clinics 19:681-705.
Ghaem O, Mellet E, Crivello F, Tzourio N, Mazoyer B, Berthoz A, Denis M (1997) Mental navigation along memorized routes activates the hippocampus, precuneus, and insula. Neuroreport 8:739-744.
Goldberg II, Harel M, Malach R (2006) When the Brain Loses Its Self: Prefrontal Inactivation during Sensorimotor Processing. Neuron 50:329-339.
Grimaldi G, Manto M (2010) Neurological Tremor: Sensors, Signal Processing and Emerging Applications. Sensors 10:1399-1422.
Hagert E (2010) Proprioception of the Wrist Joint: A Review of Current Concepts and Possible Implications on the Rehabilitation of the Wrist. Journal of Hand Therapy 23:2-17.
Haller S, Chapuis D, Gassert R, Burdet E, Klarhöfer M (2009) Supplementary motor area and anterior intraparietal area integrate fine-graded timing and force control during precision grip. European Journal of Neuroscience 30:2401-2406.
Harish K, Rao MV, Borgohain R, Sairam A, Abhilash P (2009) Tremor quantification and its measurements on parkinsonian patients. CORD Conference Proceedings 1-3.
Hendelman W (2006) Atlas of functional neuroanatomy: CRC Taylor & Francis.
Hidler J, Mbwana J, Zeffiro T (2005) MRI Compatible Force Sensing System for Real-Time Monitoring of Wrist Moments during fMRI Testing. In: 9th International Conference on Rehabilitation Robotics, pp 212-214 Chicago, IL, USA.
Hribar A, Koritnik B, Munih M (2009) Phantom haptic device upgrade for use in fMRI. Medical and Biological Engineering and Computing 47:677-684.
Hutchison WD, Lang AE, Dostrovsky JO, Lozano AM (2003) Pallidal neuronal activity: Implications for models of dystonia. Annals of Neurology 53:480-488.
Klarhöfer M, Haller S, Chapuis D, Gassert R, Roche A, Scheffler K, Burdet E, (2007) An MR-Compatible Haptic Device for fMRI Investigations of Force Control In: 15th International Society for Magnetic Resonance in Medicine, p 1965.
Kording KP, Wolpert DM (2004) Bayesian integration in sensorimotor learning. Nature 427:244-247.
Kringelbach ML (2005) The human orbitofrontal cortex: linking reward to hedonic experience. Nat Rev Neurosci 6:691-702.
Louis ED, Ferreira JJ (2010) How common is the most common adult movement disorder? Update on the worldwide prevalence of essential tremor. Movement disorders : official journal of the Movement Disorder Society 25:534-541.
Lozano AM, Kumar R, Gross RE, Giladi N, Hutchison WD, Dostrovsky JO, Lang AE (1997) Globus pallidus internus pallidotomy for generalized dystonia. Movement Disorders 12:865-870.
Maguire EA, Mummery CJ (1999) Differential modulation of a common memory retrieval network revealed by positron emission tomography. Hippocampus 9:54-61.
Martin JH (2003) Neuroanatomy: text and atlas: McGraw-Hill.
McRuer DT, Jex HR (1967) A Review of Quasi-Linear Pilot Models. Human Factors in Electronics, IEEE Transactions on HFE-8:231-249.
Mugge W, Schuurmans J, Schouten AC, van der Helm FCT (2009) Sensory Weighting of Force and Position Feedback in Human Motor Control Tasks. The Journal of Neuroscience 29:5476-5482.
Nielsen FA (2003) The Brede database: a small database for functional neuroimaging. In: 9th International Conference on Functional Mapping of the Human Brain, vol. 19 New York.
Oldfield RC (1971) The assessment and analysis of handedness: The Edinburgh inventory. Neuropsychologia 9:97-113.
Peller M, Zeuner KE, Munchau A, Quartarone A, Weiss M, Knutzen A, Hallett M, Deuschl G, Siebner HR (2006) The basal ganglia are hyperactive during the discrimination of tactile stimuli in writer's cramp. Brain 129:2697-2708.
Pintelon R, Schoukens J (2001) System Identification: a frequency domain approach. New York: IEEE Press.
Pockett S, Banks WP, Gallagher S (2006) Does consciousness cause behavior?: MIT Press.
Rascol O, Sabatini U, Fabre N, Brefel C, Loubinoux I, Celsis P, Senard JM, Montastruc JL, Chollet F (1997) The ipsilateral cerebellar hemisphere is overactive during hand movements in akinetic parkinsonian patients. Brain 120:103-110.
Rubchinsky LL, Kuznetsov AS, Wheelock VL, Sigvardt KA (2007) Tremor. Scholarpedia 2:1379.
Seger CA, Cincotta CM (2005) The Roles of the Caudate Nucleus in Human Classification Learning. The Journal of Neuroscience 25:2941-2951.
Shergill SS, Bays PM, Frith CD, Wolpert DM (2003) Two eyes for an eye: the neuroscience of force escalation. Science 301:187-187.

Thickbroom GW, Phillips BA, Morris I, Byrnes ML, Mastaglia FL (1998) Isometric force-related activity in sensorimotor cortex measured with functional MRI. Experimental Brain Research 121:59-64.
Thulborn KR (1999) Visual feedback to stabilize head position for fMRI. Magnetic Resonance in Medicine 41:1039-1043.
Tsekos NV, Khanicheh A, Christoforou E, Mavroidis C (2007) Magnetic Resonance–Compatible Robotic and Mechatronics Systems for Image-Guided Interventions and Rehabilitation: A Review Study. Annual Review of Biomedical Engineering 9:351-387.
Turner RS, Grafton ST, McIntosh AR, DeLong MR, Hoffman JM (2003) The functional anatomy of parkinsonian bradykinesia. NeuroImage 19:163-179.
Vaillancourt DE, Thulborn KR, Corcos DM (2003) Neural Basis for the Processes That Underlie Visually Guided and Internally Guided Force Control in Humans. Journal of Neurophysiology 90:3330-3340.
Van Beers RJ, Baraduc P, Wolpert DM (2002) Role of uncertainty in sensorimotor control. Philosophical Transactions of the Royal Society of London Series B: Biological Sciences 357:1137-1145.
Vitek JL, Chockkan V, Zhang J-Y, Kaneoke Y, Evatt M, DeLong MR, Triche S, Mewes K, Hashimoto T, Bakay RAE (1999) Neuronal activity in the basal ganglia in patients with generalized dystonia and hemiballismus. Annals of Neurology 46:22-35.
Volz KG, Schubotz RI, Cramon DYv (2005) Variants of uncertainty in decision-making and their neural correlates. Brain Research Bulletin 67:403-412.
Wu T, Hallett M (2005) A functional MRI study of automatic movements in patients with Parkinson's disease. Brain 128:2250-2259.
Yu H, Sternad D, Corcos DM, Vaillancourt DE (2007) Role of hyperactive cerebellum and motor cortex in Parkinson's disease. NeuroImage 35:222-233.

Appendix A: Design of fMRI compatible torque sensor

Design of torque sensor

Force sensors measure deformation of a body to which an unknown load is applied. A force sensor thus consists of a deformable body and a deformation sensor and both components need to be MR-compatible. The two main design criteria were:

- The presence of the torque sensor in the MR scanner room should not pose any danger to patients or personnel and equipment should not be damaged.
- The torque sensor should not affect the quality of the MR images and the quality of the torque sensor signal should not be affected by the MR scanner. These criteria should be met for any MR scanner with any strength of magnetic field.

To meet these criteria, a solution free of conductive and magnetic materials was selected. The used material for the deformable body was plastic, since it is easy to machine and MR-compatible. A disadvantage of plastic is its hysteretic force-deformation characteristic. The deformable body of the torque sensor was designed to be compliant in 1 direction with low cross-sensitivity by using a hub-spoke topology. Rapid prototyping, more specifically selective laser sintering, was used to manufacture the torque sensor in a short time while allowing for complex structures with high dimensional accuracy. The selected material was polyamide 12.

Deformation of the body was measured by means of a light intensity measurement. By emitting light on a surface and measuring the reflection. Due to the limited design time a commercially available optical sensor was selected. The sensor head (Keyence FU-38, see Figure A1) is made entirely from polymers and is equipped with two optical fibers (emitting and receiving) with a length of 5 m. This length was insufficient to get from the MR scanner bed to the MR control room. The optical fibers were therefore elongated to 10 m using optical couplers. To generate, receive and convert the light to an electrical signal an optical converter is used (Keyence FS-N11MN) which has a 1 to 5 V voltage output proportional to the received light intensity, a repeat precision of 0.5% FS and a 1ms response time.

Figure A1 Optical head by Keyence (FU-38)

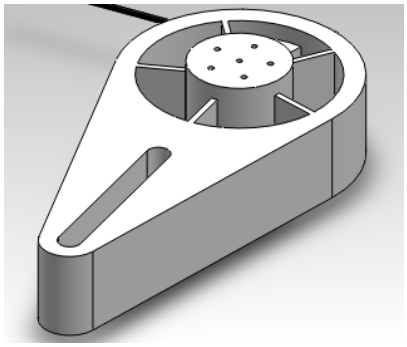

Figure A2 Design of deformable body

The design of the torque sensor is shown in Figure A2. The slot allows for fixation of a handgrip at various distances to accommodate a wide range of hand sizes. The deformable body was designed such that when a torque of 1.2Nm is applied, the sensor head mounted on the outer rim will displace 125 µm (in the x-direction, see Figure A3) with respect to the reflective surface attached to the hub. A more detailed view of the reflective surface and its adjustment mechanism are depicted in Figure A3. The adjustment mechanism was necessary to set the electrical output of the optical converter to 50% when no torque was applied, allowing for torque measurement in two directions.

The sensor was mounted in a test setup for calibration and initial testing. The maximum detectable torque level was 1.5 Nm. To test the repeatability of the assembled sensor four torques were repeatedly applied in random order. Table A1 shows the mean and standard deviations of the measured values. These results were acquired with the original optical fiber length of 5 m.

Table A1 Measured torques (mean and standard deviation)

Applied torque [Nm]	Measured torque (mean and sd) [Nm]	Number of repetitions [-]
0.4280	0.4503 (0.0045)	3
0.6504	0.6542 (0.0148)	3
0.8997	0.9034 (0.0044)	4
1.2288	1.2086 (0.0074)	3

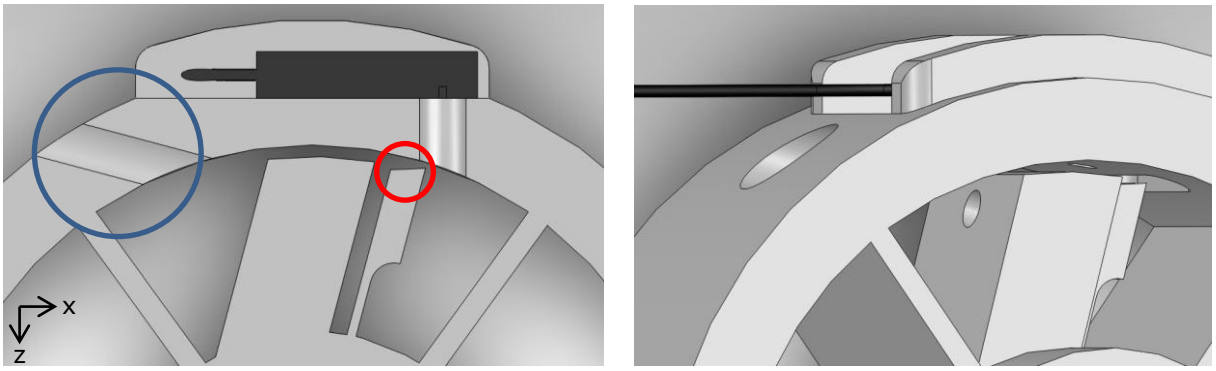

Figure A3 Adjustment mechanism (left: section view, right: 3d view). The optical sensor (black) emits light on the reflective surface (top of element on thin beam, circled in red). Inserting a nylon screw through the hole in the rim (circled in blue) and in the threaded thick element (to the left of the thin beamed structure) allowed for adjustment of the reflective surface to get 50% intensity at zero applied torque.

Design of sensor mount

The design criteria for the sensor mount were the same as those mentioned for the sensor and additionally included:

- The sensor mount should counteract flexion/extension wrist torque
- The torque sensor should be fixed with respect to forearm
- Space on arm should be available to accommodate EMG electrodes for future purposes
- Muscles in forearm (for flexion/extension of wrist) should not be restricted

The designed torque sensor needed to be fixed with respect to the forearm to allow for isometric torque measurement of the wrist. This fixation can be achieved by installing the torque sensor in the MR scanner room and strap the forearm of the subject in; alternatively, the torque sensor can be attached to the forearm of the subject. Advantages of the second option include: reduced installation time inside the MR scanner room since the sensor mount can be attached to the subject outside the MR scanner room, and less head motion since the subject exerts no force to his surroundings. The torque sensor was mounted on a milled polyoxymethylene adapter block. This block also houses a plastic wrist support and a fiberglass rod, capsuled in a shrinking tube, to connect the block to the lower arm support around the elbow. Moldable foam (polypropylene), plastic straps (for comfort and filling), and Velcro straps are used to fixate a subject's arm in the sensor mount. The foam becomes moldable when moistened and quickly hardens out again. Adjusting the shape of the foam and the number of plastic straps allowed for fixation of a wide range of arm sizes. The assembled torque sensor is shown in Figure A4.

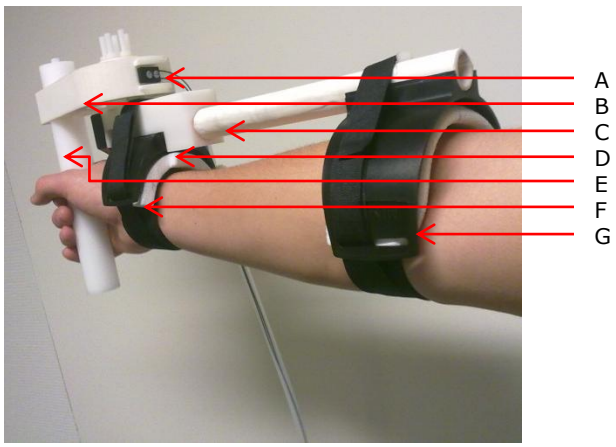

Figure A4 The assembled torque sensor attached to the lower arm. Indicated in the figure: light intensity sensor with 10m optical fiber [A], polyamide 12 deformable body [B], fiberglass rod [C], polyoxymethylene mounting block [D], polyoxymethylene handle [E] and plastic armrests [F&G] with moldable foam and Velcro straps.

Performance of the torque sensor

As mentioned the optical fibers were too short to be able to place the optical converter outside the MR scanner room. Unfortunately the sensor head was not available with longer optical fibers, which left elongation as the only option. Optical couplers (Keyence FU-C1) were used to attach another 5 m of optical fiber resulting in a total optical fiber length of 10m. The optical fiber was placed inside a polyethylene tube for protection. The use of couplers inevitably resulted in signal loss, which could to a limited extent be compensated for by altering the settings of the optical converter. The resulting response time of the optical converter was 4.2 ms. A disadvantage of the sensor is its sensitivity to creep, which is inherent to the use of a polymer for the deformable body.

Appendix B: Images presented to subject during instruction time

The following images were shown to the subject during 5 seconds. There was a countdown timer in the center of the screen that counted back from 5 seconds to 1 second.

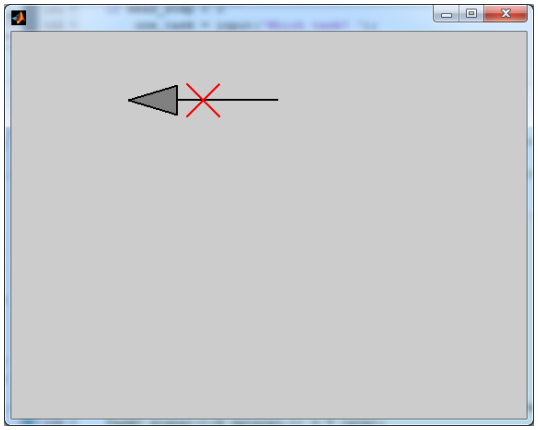

Task 1: rest

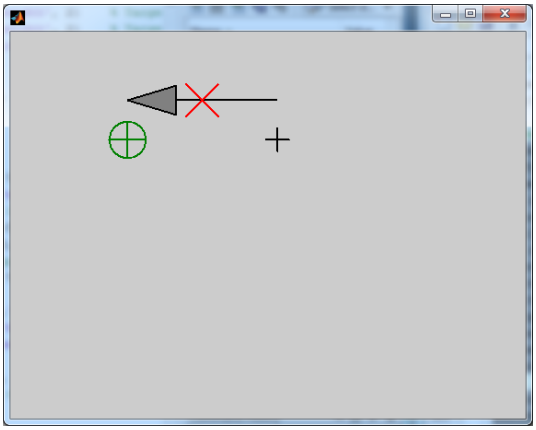

Task 2: rest with visual stimulus

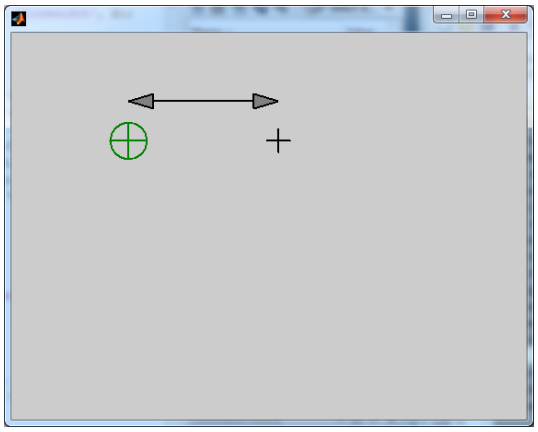

Task 3: Fast switching torque task with visual feedback

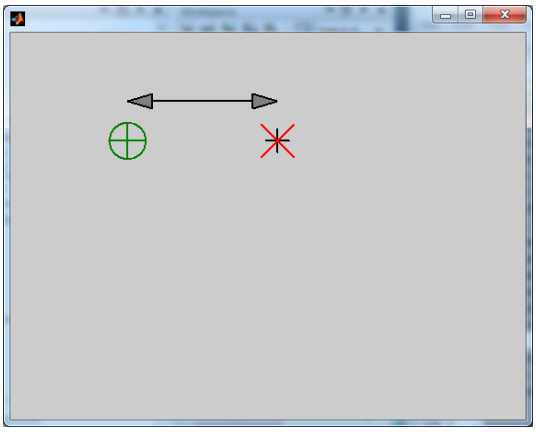

Task 4: Fast switching torque task without visual feedback

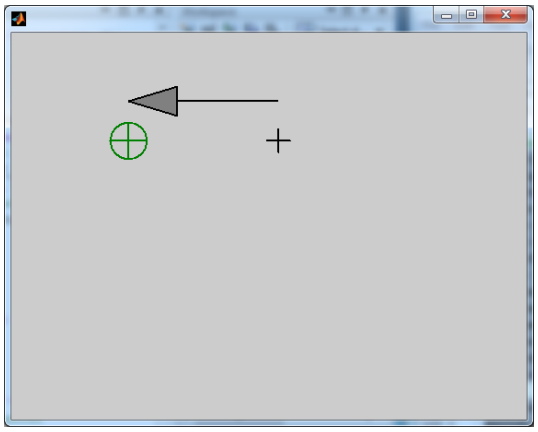

Task 5: constant torque with visual feedback

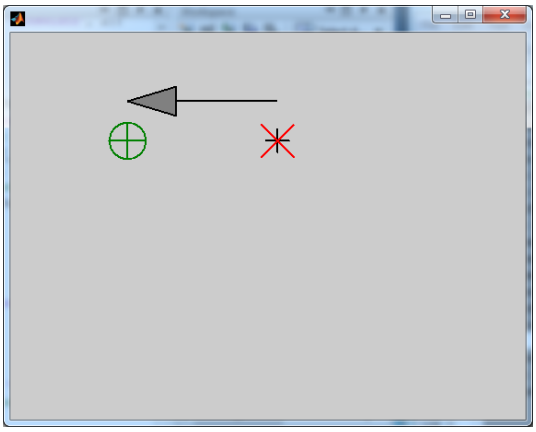

Task 6: constant torque without visual feedback

Task 7: constant torque with visual disturbance

Appendix C: Image data flow for processing scans using SPM8

This appendix describes the actions performed using SPM8 to achieve the presented results.

The following steps are taken:

1. Anatomical realignment of all 356 functional scans to the first functional scan, which is performed to reduce the effects of head movement. Realignment ensures that brain structures remain in the same position over time, which is necessary for correct analysis (see Figure C1). The movement parameters extracted from realignment are stored for later use.
2. Coregistration of all functional scans to the anatomical scan to achieve alignment (see Figure C1).
3. Normalization of functional scans to MNI template is performed to enable group analysis. The purpose of the high resolution anatomical scan is that it can be accurately warped to the MNI template using segmentation of white and grey matter. Since the functional scans are coregistered with the anatomical scan, they can undergo the same manipulations as the anatomical scan to achieve normalization (see Figure C1).
4. Smoothing of functional scans is performed to account for small anatomical differences between subjects and to improve the signal-to-noise ratio.
5. The design matrix (general linear model) is specified by entering all events (warm-up, task instructions and tasks) in the model using their onsets and durations (see Figure C2). These regressors are convolved with the hemodynamic response function. The movement parameters are entered as extra regressors.
6. The parameters are estimated by minimizing the sum of squared residuals.
7. The design matrix is verified to be orthogonal for the regressors of interest.
8. Per subject contrasts are specified for all comparisons (5vs6, 6vs5, 3vs4, 4vs3, 5vs7, 7vs5)
9. The group analysis is performed using a one sample t-test on the five (one for each subject) contrast images for each of the comparisons (5vs6, 6vs5, 3vs4, 4vs3, 5vs7, 7vs5).

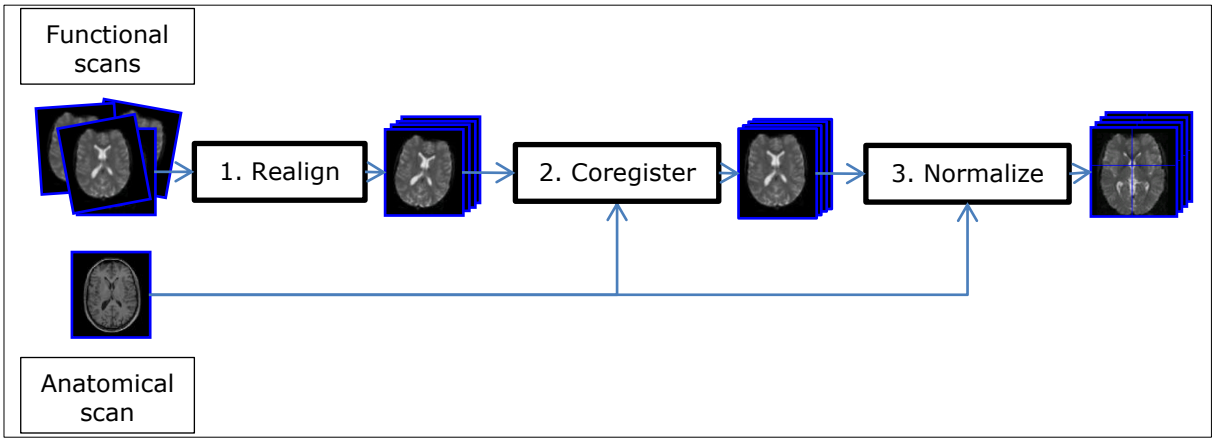

Figure C1 The first three steps of processing. See text for explanation. (Adapted from the SPM8 homepage: http://www.fil.ion.ucl.ac.uk/spm).

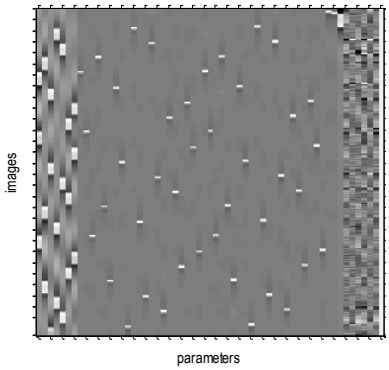

Figure C2 Example of a design matrix for a subject. The regressors are on the horizontal axis and the 356 scans are on the vertical axis (1 to 356 from top to bottom). The first 7 columns are the regressors for the 7 tasks. The grey columns at the far right are the movement parameters extracted from realignment (step 1).

A very short and oversimplified explanation of the statistical analysis will be presented, which is for a large part derived from the SPM8 homepage (http://www.fil.ion.ucl.ac.uk/spm).

The general linear model (Y = X β + ε) is used for each individual voxel, under the assumption that $\varepsilon \sim N(0, \sigma^2)$. Here, Y is a 1xN (N=number of scans) vector containing the measurement data, X is the PxN (P=number of regressors) design matrix that is convolved with the hemodynamic response function), β is a 1xP parameter vector that is to be estimated and ε is a 1xN vector representing the error. The parameter vector is estimated ($\hat{\beta}$) by ordinary least squares estimation: $\hat{\beta} = (X^T X)^{-1} X^T Y$. Then $\hat{\varepsilon} = Y - X\hat{\beta}$, and the residual for each voxel, $\hat{\sigma}_i^2 = \frac{\hat{\varepsilon}^T \hat{\varepsilon}}{N-P}$, is a measure for the 'goodness of the fit' and is used in the statistical analysis. Once β is estimated (for each voxel), contrasts can be generated by combining the relevant terms from β. If for example the goal is to test if there is increased activity during task 1 compared to task 2, the following contrast vector (Px1) is used: c=[1 -1 0 0 0 …]. The β terms are combined to produce relevant contrast values: $c^T \beta$. These contrast values are generated for each voxel in each subject, leading to one map per subject containing the contrast values for each scanned voxel in the brain.

These contrast maps can be tested using the following t-test for each voxel: $T = \frac{c^T \hat{\beta}}{\sqrt{var(c^T \hat{\beta})}} = \frac{c^T \hat{\beta}}{\sqrt{\hat{\sigma}_i^2 c^T (X^T X)^{-1} c}}$. The result of the individual analysis is a map with a T value for each voxel. When thresholding the map of T values for a contrast, the voxels with a T value higher than the threshold will be regarded as significant, under the null hypothesis H_0 that there is no effect. These voxels can be projected on a brain image to perform further analysis.

When performing a group analysis for a specific contrast, the contrast maps ($c^T \hat{\beta}$ for each voxel) for each subject are used as observations in a GLM. So again Y = X β + ε is used for each individual voxel. Here, Y is a 1xN (N=number of subjects) vector containing the contrast, X is the 1xN design matrix, β is a scalar that is to be estimated and ε is a 1xN vector representing the error. Again the sum of the squared residuals is minimized to find the value for β. The resulting β and a simple contrast vector c=[1] are used in the same t-test as before, and generates a map with a T value for each voxel.

The final step in generating the results figures is to determine an appropriate significance level. Since a large amount of t-tests is performed the multiple comparisons problem rises. A significance level of α=0.05 will result in many false positives. To account for this problem a Bonferroni correction can be applied, which tests the individual voxels at a significance level of α/n, where n is the number of performed tests (the number of voxels). However, this correction is overly conservative (increased number of false negatives), since the tested voxels are not all independent observations but can be correlated with their neighbors. Another way to account for the multiple comparison problem is to use random field theory to set an appropriate significance level that is corrected for the number of independent observations. The random field theory determines the numbers of resels (resolution elements) in an image, determines the expected Euler characteristic of the image for different threshold levels and uses this characteristic to determine an appropriate threshold. A more detailed explanation can be found at http://imaging.mrc-cbu.cam.ac.uk/imaging/PrinciplesRandomFields. An important limitation of the random field theory is that it requires sufficient smoothness of the T-map and requires even higher smoothness for a T-map with few degrees of freedom, where degrees of freedom is defined as the number of images minus the number of regressors. So for a group analysis with only few subjects (hence a few degrees a freedom) as is the case in this study, the random field theory is suboptimal and more specifically results in a high number of false negatives.

In this study an uncorrected significance level of α=0.001 is chosen with a minimum cluster extent of 5 clusters, which is a common combination in literature to control for false positives and false negatives.

Appendix D: Detailed fMRI results

The following data was produced using the xjView8.4 toolbox[1]. The first line is the cluster number. The active clusters are ordered from bottom to top in the sagittal plane in Figure 4 to Figure 6. The second line shows the coordinates where the clusters are located in the MNI brain. The third line shows the maximum T value in the cluster, resulting from the statistical analysis. T>7.1732 was considered significant (p=0.001) and a 5 voxel extent threshold was used. The middle section gives the specific brain region and how many voxels were found to be active in this region. A voxel can belong to multiple brain regions. Total number of clusters (TOTAL) is only shown when it is different from the first mentioned brain region. The bottom line shows the region that is believed to be the main component of the active cluster of voxels. When xjview8.4 did not result in a specific brain region, AAL[2] was consulted.

Results for 5vs6

19 clusters of active voxels were found.

Cluster 1 6 -82 -39 Tmax=14.5587	Cluster 2 -44 -10 -35 Tmax=13.9469	Cluster 3 -30 -52 -35 Tmax=10.8006	Cluster 4 30 -46 -33 Tmax=26.6595	Cluster 5 26 -56 -23 Tmax=14.5375
17 TOTAL 12 CBL_Crus2_R 10 Right CBL 10 CBL Posterior Lobe 5 Uvula 5 Pyramis 2 CBL_7b_R	13 TOTAL 11 Left CB 11 Temporal Lobe 11 Inferior Temporal Gyrus 9 Temporal_Inf_L 9 brodmann 20 9 Gray Matter	10 Left CBL 9 CBL Anterior Lobe 3 CBL_6_L 1 Tuber 1 CBL Posterior Lobe	9 Right CBL 9 CBL Anterior Lobe 7 Culmen 6 CBL_6_R	16 Right CBL 16 CBL_6_R 10 CBL Posterior Lobe 10 Declive 6 Culmen 6 CBL Anterior Lobe
CBL Posterior Lobe	Inferior Temporal Gyrus	CBL Anterior Lobe	CBL Anterior Lobe	CBL Posterior & Anterior lobe

Cluster 6 42 -62 -13 Tmax=8.8839	Cluster 7 -26 -90 -9 Tmax=23.6571	Cluster 8 -42 -84 -5 Tmax=10.8161	Cluster 9 44 -86 -5 Tmax=19.4918	Cluster 10 -20 0 11 Tmax=12.0314
17 White Matter 17 Right CB 16 Sub-Gyral 9 Occipital Lobe 8 Temporal Lobe 5 Occipital_Inf_R 5 Temporal_Inf_R 3 Temporal_Mid_R 1 Middle Temporal Gyrus 1 Fusiform_R	31 Left CB 31 Occipital Lobe 31 Occipital_Inf_L29 White Matter 18 Inferior Occipital Gyrus 11 Sub-Gyral 2 Lingual Gyrus 2 brodmann 18 2 Gray Matter	12 Left CB 12 Occipital Lobe 12 Occipital_Inf_L 10 White Matter 9 Inferior Occipital Gyrus 2 Gray Matter 2 brodmann 19 2 Middle Occipital Gyrus 1 Sub-Gyral	29 Occipital Lobe 29 Right CB 28 Occipital_Inf_R 20 White Matter 16 Middle Occipital Gyrus 13 Inferior Occipital Gyrus 9 Gray Matter 5 brodmann 18 4 brodmann 19 1 Occipital_Mid_R	13 Gray Matter 13 Left CB 13 Lentiform Nucleus 13 Sub-lobar 12 Putamen 8 Putamen_L 3 Pallidum_L 1 Lateral Globus Pallidus
Occipital Lobe	Occipital Lobe	Occipital Lobe	Occipital Lobe	Putamen

[1] xjView toolbox (http://www.alivelearn.net/xjview)

[2] Automated Anatomical Labeling of Activations in SPM Using a Macroscopic Anatomical Parcellation of the MNI MRI Single-Subject Brain. N. Tzourio-Mazoyer, B. Landeau, D. Papathanassiou, F. Crivello, O. Etard, N. Delcroix, B. Mazoyer, and M. Joliot. NeuroImage 2002. 15 :273-289
http://www.cyceron.fr/web/aal__anatomical_automatic_labeling.html

Cluster 11 66 -52 7 Tmax=18.044	Cluster 12 50 -62 11 Tmax=8.9616	Cluster 13 -24 -84 13 Tmax=12.9858	Cluster 14 -32 -42 49 Tmax=15.0543	Cluster 15 -36 -10 51 Tmax=15.1314
11 Right CB 11 Temporal Lobe 11 Temporal Mid_R (aal) 10 Superior Temporal Gyrus 7 Gray Matter 6 brodmann 22 4 White Matter 1 Middle Temporal Gyrus 1 brodmann 21	6 Middle Temporal Gyrus 6 Right CB 6 Temporal Mid_R (aal) 3 Gray Matter 3 Temporal Lobe 3 Occipital Lobe 3 White Matter 3 brodmann 19	9 Left CB 9 Middle Occipital Gyrus 9 Occipital Lobe 9 Occipital_Mid_L 9 White Matter	20 Left CB 20 Parietal Lobe 20 White Matter 14 Parietal_Inf_L 14 Sub-Gyral 5 Postcentral_L 4 Inferior Parietal Lobule 2 Postcentral Gyrus 1 Parietal_Sup_L (aal)	10 Frontal Lobe 10 Left CB 10 Precentral_L 9 Precentral Gyrus 5 brodmann 6 5 Gray Matter 4 White Matter 1 Middle Frontal Gyrus
Superior Temporal Gyrus	Middle Temporal Gyrus	Occipital Lobe	Inferior Parietal Lobule	Precentral gyrus

Cluster 16 42 4 51 Tmax=11.92	Cluster 17 -20 -14 59 Tmax=54.9395	Cluster 18 38 0 61 Tmax=9.5904	Cluster 19 -26 -22 65 Tmax=11.2451
5 Frontal Lobe 5 Frontal_Mid_R 5 Middle Frontal Gyrus 5 Right CB 5 White Matter	65 Left CB 65 Frontal Lobe 40 White Matter 30 Sub-Gyral 25 Precentral_L 24 Middle Frontal Gyrus 20 brodmann 6 20 Gray Matter 7 Frontal_Sup_L 6 Superior Frontal Gyrus 4 Supp_MotorArea_L 4 Precentral Gyrus 1 Medial Frontal Gyrus	20 Frontal Lobe 20 Frontal_Mid_R (aal) 20 Middle Frontal Gyrus 20 Right CB 19 White Matter 1 brodmann 6 1 Gray Matter	7 Frontal Lobe 7 Left CB 7 Precentral Gyrus 7 Precentral_L 7 White Matter
Middle Frontal Gyrus	Precentral gyrus	Middle Frontal Gyrus	Precentral Gyrus

Results for 6vs5
4 clusters of active voxels were found.

Cluster 1 -20 -94 15 Tmax=12.0945	Cluster 2 16 -92 15 Tmax=11.746	Cluster 3 38 -16 21 Tmax=15.6705	Cluster 4 8 -14 31 Tmax=10.9963
9 Left CB 9 Occipital Lobe 9 Occipital_Mid_L 6 Gray Matter 6 Middle Occipital Gyrus 6 brodmann 18 3 White Matter 3 Cuneus	9 Cuneus 9 Occipital Lobe 9 Right CB 7 White Matter 4 Occipital_Sup_R 4 Cuneus_R 2 brodmann 19 2 Gray Matter 1 Calcarine_R	12 Sub-lobar 12 Right CB 10 White Matter 9 Insula 5 Rolandic_Oper_R 4 Insula_R 3 Extra-Nuclear 2 brodmann 13 2 Gray Matter	5 Limbic Lobe 5 Right CB 5 White Matter 5 Cingulate Gyrus 3 Cingulum_Mid_R
Occipital Lobe	Occipital Lobe	Insula	Cingulate Gyrus

Results for 3vs4
5 clusters of active voxels were found.

Cluster 1 24 -92 -1 Tmax=13.8277	Cluster 2 -34 -78 3 Tmax=22.1826	Cluster 3 22 8 17 Tmax=14.0931	Cluster 4 -58 -8 41 Tmax=11.4131	Cluster 5 26 -42 49 Tmax=9.0344
6 Occipital Lobe 6 Occipital_Inf_R 6 Right CB 4 Middle Occipital Gyrus 4 White Matter 2 Gray Matter 2 brodmann 18 2 Sub-Gyral	10 Left CB 10 Middle Occipital Gyrus 10 Occipital Lobe 10 Occipital_Mid_L 10 White Matter	9 Right CB 9 Sub-lobar 9 White Matter 9 Extra-Nuclear 2 Caudate_R	6 Frontal Lobe 6 Left CB 6 Postcentral_L 6 Precentral Gyrus 5 White Matter 1 brodmann 6 1 Gray Matter	7 Right CB 7 Sub-Gyral 7 White Matter 7 Parietal Lobe 3 Postcentral_R
Occipital Lobe	Occipital lobe	Caudate nucleus AAL:34% caudate	Postcentral Gyrus & Precentral Gyrus	Postcentral gyrus

Results for 4vs3
8 clusters of active voxels were found.

Cluster 1 -28 -18 -31 Tmax=13.796	Cluster 2 24 -14 -23 Tmax=24.0554	Cluster 3 -20 -14 -25 Tmax=7.811	Cluster 4 8 48 -7 Tmax=22.3729	Cluster 5 -10 52 -9 Tmax=16.6605
13 TOTAL 12 Limbic Lobe 12 Parahippocampal Gyrus 12 Left CB 8 White Matter 7 ParaHippocampal_L 6 Fusiform_L 4 Gray Matter 3 brodmann 36 1 brodmann 35	23 Limbic Lobe 23 Parahippocampal Gyrus 23 Right CB 19 ParaHippocampal_R 11 Gray Matter 9 White Matter 5 brodmann 35 4 Hippocampus_R 4 brodmann 28 2 brodmann 34	6 TOTAL 5 Limbic Lobe 5 Parahippocampa Gyrus 5 Left CB 4 Gray Matter 4 brodmann 28 4 ParaHippocampal_L 1 Hippocampus_L 1 White Matter	40 TOTAL 39 Right CB 37 Frontal Lobe 36 Frontal_Med_Orb_R 32 White Matter 27 Medial Frontal Gyrus 8 Sub-Gyral 5 Gray Matter 3 brodmann 10 2 brodmann 11 2 Superior Frontal Gyrus 1 Frontal_Sup Orb_R 1 Inter-Hemispheric	19 Left CB 18 White Matter 18 Frontal Lobe 12 Frontal_Med_Orb_L 9 Medial Frontal Gyrus 7 Sub-Gyral 2 Superior Frontal Gyrus 1 Gray Matter 1 Anterior Cingulate 1 Limbic Lobe 1 brodmann 32 1 Cingulum_Ant_L
Parahippocampal Gyrus	Parahippocampal Gyrus	Parahippocampal Gyrus	Frontal orbital lobe	Frontal orbital lobe

Cluster 6 14 10 31 Tmax=17.8071	Cluster 7 -54 -60 31 Tmax=12.3223	Cluster 8 -22 38 49 Tmax=10.3696
6 Limbic Lobe 6 Right CB 6 White Matter 6 Cingulate Gyrus	7 Left CB 7 Parietal Lobe 6 Supramarginal Gyrus 5 Gray Matter 4 brodmann 40 4 Angular_L 2 White Matter 1 Angular Gyrus 1 brodmann 39	6 Frontal Lobe 6 Frontal_Sup_L 6 Gray Matter 6 Left CB 6 brodmann 8 3 Superior Frontal Gyrus 3 Middle Frontal Gyrus
Cingulate Gyrus	Supramarginal Gyrus	brodmann area 8

Results for 7vs5
6 clusters of active voxels were found.

Cluster 1 -8 -46 -33 Tmax=17.0554	Cluster 2 16 -42 -31 Tmax=17.4436	Cluster 3 52 -12 -11 Tmax=11.4915	Cluster 4 -16 38 11 Tmax=15.3828	Cluster 5 -6 36 47 Tmax=10.4227
18 Left CBL18 CBL Anterior Lobe 13 CBL_9_L 4 Nodule 2 Dentate	12 Right CBL 12 CBL Anterior Lobe 3 CBL_9_R 3 Dentate	8 Right CB 8 Temporal Lobe 8 White Matter 6 Middle Temporal Gyrus 4 Temporal_Mid_R 4 Temporal_Sup_R 2 Sub-Gyral	6 Left CB 5 White Matter 4 Frontal Lobe 4 Sub-Gyral 2 Limbic Lobe 2 Anterior Cingulate 1 brodmann 32 1 Gray Matter	7 Frontal Lobe 7 Frontal_Sup_Medial_L 7 Left CB 6 Gray Matter 6 brodmann 8 4 Superior Frontal Gyrus 3 Medial Frontal Gyrus 1 White Matter
CBL Anterior Lobe	CBL Anterior Lobe	Middle and Superior Temporal Gyrus	Anterior cingulate	brodmann area 8

Cluster 6 -16 -2 59 Tmax=13.5825
12 Left CB 12 Frontal Lobe 11 White Matter 7 Sub-Gyral 5 Medial Frontal Gyrus 1 brodmann 6 1 Gray Matter
Medial Frontal Gyrus AAL:34% Supplementary motor area